Controlling the Zero Hall Plateau in a Quantum Anomalous Hall Insulator by In-Plane Magnetic Field

Jianli Luan,[1,*] Yang Feng,[2,*] Yuchen Ji,[3,*] Yuanzhao Li,[1] Hangzhe Li,[1] Zhongkai Liu,[3] Chang Liu,[2] Jinsong Zhang,[1,5,6] Xufeng Kou,[3,4,†] and Yayu Wang[1,5,6,‡]

[1]*State Key Laboratory of Low Dimensional Quantum Physics, Department of Physics, Tsinghua University, Beijing 100084, People's Republic of China*
[2]*Beijing Academy of Quantum Information Sciences, Beijing 100193, People's Republic of China*
[3]*ShanghaiTech Laboratory for Topological Physics, School of Physical Science and Technology, ShanghaiTech University, Shanghai 201210, People's Republic of China*
[4]*School of Information Science and Technology, ShanghaiTech University, Shanghai 20031, People's Republic of China*
[5]*Frontier Science Center for Quantum Information, Beijing 100084, People's Republic of China*
[6]*Hefei National Laboratory, Hefei 230088, People's Republic of China*

(Received 27 August 2022; accepted 7 April 2023; published 1 May 2023)

We investigate the quantum anomalous Hall plateau transition in the presence of independent out-of-plane and in-plane magnetic fields. The perpendicular coercive field, zero Hall plateau width, and peak resistance value can all be systematically controlled by the in-plane magnetic field. The traces taken at various fields almost collapse into a single curve when the field vector is renormalized to an angle as a geometric parameter. These results can be explained consistently by the competition between magnetic anisotropy and in-plane Zeeman field, and the close relationship between quantum transport and magnetic domain structure. The accurate control of zero Hall plateau facilitates the search for chiral Majorana modes based on the quantum anomalous Hall system in proximity to a superconductor.

DOI: 10.1103/PhysRevLett.130.186201

The discovery of the quantum anomalous Hall (QAH) effect in magnetic topological insulator (TI) opens a new route for studying novel topological phases of quantum matter [1–7]. From the fundamental physics point of view, a key issue is whether there are phases and phase transitions that are exclusive to the QAH effect due to the interplay of topology and magnetism. In this regard, the transition between the QAH plateaus with the Chern number $C = +1$ and $C = -1$ has attracted particular attention because it is driven by magnetization reversal instead of the Landau level occupation like in the conventional quantum Hall effect. It has been theoretically proposed that the QAH plateau transition can be mapped to the Chalker-Coddington network model for the integer quantum Hall plateau transition [8,9]. Because of the quantum percolation through a network of chiral edge states, in which tunneling at the saddle point dominates the critical behavior, an intermediate zero Hall plateau (ZHP) with $C = 0$ is expected to exist. Experimentally, a zero Hall conductance ($\sigma_{xy} = 0$) plateau has indeed been observed in QAH systems around the coercive field [10,11]. However, different types of QAH thin films exhibit distinct ZHP behaviors as functions of magnetic field and temperature, and there are inconsistencies between theoretical prediction and experimental observations [12–15].

The ZHP has aroused more interest recently because it is expected to play a pivotal role in the search for chiral Majorana modes in QAH-based heterostructure [16]. It has been proposed that during the transition from the $C = 1$ to the $C = 0$ plateau for a QAH film in proximity to an s-wave superconductor (SC), there exists a chiral topological SC phase with a half-integer quantized conductance plateau with $C = 1/2$. Despite the report of the $C = 1/2$ plateau in a QAH film covered by a Nb strip [17], there are debates regarding the validity of the claim for the existence of chiral Majorana modes [18–20]. In order to optimize the realization of chiral Majorana fermions in a QAH-SC heterostructure, the $C = 0$ phase must fulfill the following requirements. First, the $C = 1$ and $C = 0$ plateaus should both be well developed, rather than the anticorrelation between them as observed previously [10]. Second, the magnetic field scale for the plateau transition should be as low as possible, so that the fragile proximity induced topological SC is not suppressed. Third, the transition should be smooth and broad, so there is a large parameter space for the chiral topological SC phase. Last, it is highly desirable to achieve an accurate control of the plateau transition, preferable in an *in situ* manner.

In this Letter, we introduce a new method to accurately control the properties of the ZHP and its transition to the $C = 1$ plateau in a QAH insulator by applying an in-plane magnetic field. The transition field, ZHP width, and peak resistance value can all be systematically tuned by the in-plane field. The traces taken at various fields almost

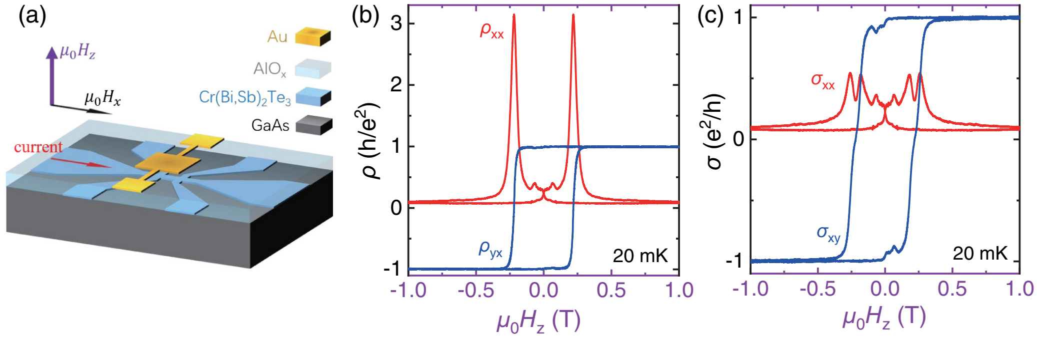

FIG. 1. (a) The schematic diagram of the device structure and measurement setup. The out-of-plane and in-plane magnetic fields are denoted by the purple and black arrows, respectively. (b) Hysteresis loops of longitudinal resistivity ρ_{xx} and Hall resistivity ρ_{yx} as function of H_z at the optimal gate voltage $V_g = 6$ V. (c) Hysteresis loops of σ_{xx} and σ_{xy} converted from the data in (b). There is no obvious ZHP near the coercive field, and σ_{xx} only shows a shallow dip.

collapse into a single curve when the field vector is renormalized to an angle as a geometric parameter. These results can be explained consistently by the competition between magnetic anisotropy and in-plane Zeeman field, and the close relationship between quantum transport and magnetic domain structure. This new way of controlling the ZHP is highly advantageous for searching the chiral Majorana mode in a QAH-SC hybrid system.

The $Cr_{0.092}(Bi_{0.27}Sb_{0.73})_{1.908}Te_3$ film with thickness 5 QL (quintuple layer) studied here is grown by molecular beam epitaxy on a GaAs substrate, as described in previous reports [21,22]. Figure 1(a) displays the schematic device structure and measurement setup. To minimize the degradation of sample quality during fabrication, we use ion milling with molybdenum hard mask to define the Hall bar device. A top gate is fabricated on the Hall bar by depositing 40 nm thick AlO_x using atomic layer deposition followed by the evaporation of a Ti/Au electrode through another hard mask. During the transport measurement, a dc current is applied by a Keithley 6221 source meter and the voltage is detected by a Keithley 2182A voltmeter in the delta mode. A small current ~3 nA is applied to minimize the heating effect as described in Supplemental Material [23]. The perpendicular and in-plane magnetic fields are applied independently by a vector magnet.

Figure 1(b) shows the Hall resistivity ρ_{yx} and longitudinal resistivity ρ_{xx} with respect to the perpendicular magnetic field H_z, measured at the base temperature $T = 20$ mK and optimal gate voltage $V_g = 6$ V. As shown by the gate dependent transport results in Supplemental Material [23] Fig. S2, the optimal V_g is chosen to reach the maximum ρ_{xx} peak and nearly minimum residual ρ_{xx} value. It shows the typical QAH effect in which ρ_{yx} forms a quantized plateau close to h/e^2 and the residual ρ_{xx} at $\mu_0 H_z = 1$ T is lower than 0.08 h/e^2. The peak ρ_{xx} values at the coercive field H_{cz} is about 3.1 h/e^2. The coexistence of low residual ρ_{xx} value and sharp ρ_{xx} peak indicates the high sample quality with a low level of disorder [37]. When we convert the resistivity to conductivity using the tensor relation (the justification of the in-plane isotropic assumption is shown in Supplemental Material [23] Fig. S3), the Hall conductivity σ_{xy} shown in Fig. 1(c) is well quantized, but there is no obvious ZHP near H_{cz}. Instead, σ_{xy} forms a smooth shoulder and the longitudinal conductivity σ_{xx} shows a small dip at H_{cz}, both reflecting the resistive behavior during magnetization reversal.

We then study the influence of in-plane magnetic field H_x on the QAH plateau transition. Shown in Figs. 2(a) and 2(b) are the ρ_{yx} and ρ_{xx} versus H_z hysteresis loops when H_x is fixed at varied values. There are several systematic trends with increasing H_x. First, the slope of ρ_{yx} versus H_z during the plateau transition decreases, and a higher H_z is needed to realize the $C = +1$ plateau. Second, the out-of-plane coercive field H_{cz} decreases systematically and drops to zero for $\mu_0 H_x \geq 1$ T, as summarized by the purple squares in Fig. 2(c). Third, the ρ_{xx} peak value at H_{cz} shows a nonmonotonic variation. It increases up to ~13 h/e^2 for $\mu_0 H_x = 0.7$ T and then decreases gradually, as summarized by the red open circles in Fig. 2(c). The higher ρ_{xx} peaks and lower ρ_{yx} slopes lead to deeper dips in σ_{xx} and broader ZHP around H_{cz}, as revealed by Figs. 2(d) and 2(e). For $\mu_0 H_x \geq 0.3$ T, the width of the ZHP becomes quite significant, and it keeps increasing for higher H_x. Figure 2(f) displays the variation of ZHP width with H_x defined by the field range when σ_{xy} is smaller than a threshold 0.005 e^2/h. Above an onset field scale $\mu_0 H_i = 0.28$ T, the ZHP width becomes finite and then increases linearly with H_x.

Despite the development of ZHP with increasing H_x, the $C = 1$ QAH plateau is still well quantized in sufficiently high H_z (the data at larger H_z scales are shown in Supplemental Material [23] Fig. S4), thus realizing the coexistence of $C = 1$ and $C = 0$ plateaus. The evolution between the two phases can be visualized by the global phase diagram when we plot σ_{xx} as a function of σ_{xy}. As shown in Fig. 2(g), the insulating phase at points $(\sigma_{xx}, \sigma_{xy}) = (0, 0)$ becomes evident for $\mu_0 H_x \geq 0.3$ T,

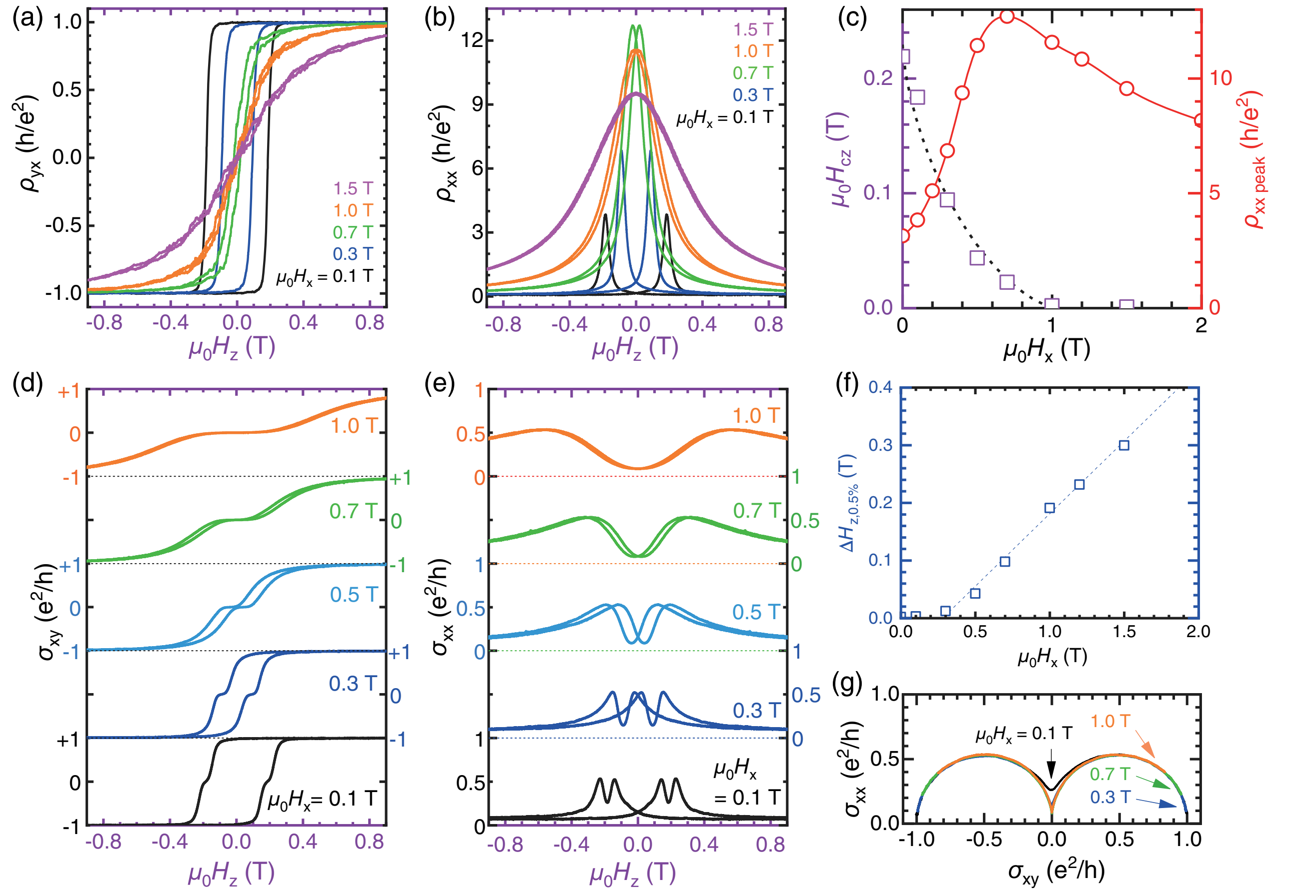

FIG. 2. (a),(b) The ρ_{xx} and ρ_{yx} versus H_z loops measured with H_x fixed at different levels. (c) The dependence of perpendicular coercivity H_{cz} and ρ_{xx} peak values on H_x. The black dashed line is the simulation based on the Stoner-Wohlfarth model described in Supplemental Material [23]. (d),(e) The σ_{xx} and σ_{xy} loops converted from the data in (a) and (b) using the tensor relation. (f) The ZHP width estimated from (d), which becomes finite from $\mu_0H_x = 0.3$ T and increases linearly above that. (g) The parametric plots show that the system approaches the insulating phase at $[\sigma_{xy}(\mu_0H_z), \sigma_{xx}(\mu_0H_z)] = (0, 0)$ with increasing μ_0H_x values.

which can also be seen directly in Figs. 2(d) and 2(e). The traces taken at different H_x values all form a semicircle with radius of $1/2\ e^2/h$ centered at ($\pm 0.5\ e^2/h$, 0), revealing three fixed points corresponding to the $C = \pm 1$ and $C = 0$ states, respectively. The slight deviation of the max σ_{xx} value from $1/2\ e^2/h$ is due to the broadening of plateau transition, and sensitive to gate voltage as shown in Supplemental Material [23] Fig. S5. The nearly identical flow trajectory for the traces taken in varied H_x values indicates the robustness of both the QAH and ZHP states, and the universal quantum criticality for the plateau transitions.

To directly illustrate the plateau transition driven by the in-plane magnetic field, we perform the H_x sweeps with fixed H_z. To eliminate the influence of magnetization history, an appropriate sequence of field sweep is adopted, as described in Supplemental Material [23]. Figures 3(a) and 3(b) display the ρ_{yx} and ρ_{xx} versus H_x loops for $\mu_0H_z = 0.1$, 0.2, and 0.3 T, respectively. For each fixed H_z, the system shows the typical QAH behavior at $\mu_0H_x = 0$ T with a quantized ρ_{yx} and nearly vanishing ρ_{xx}. With increasing H_x, ρ_{yx} first remains at the $C = 1$ plateau and is then gradually suppressed, which is accompanied by the deviation of ρ_{yx} from zero. These behaviors indicate the destruction of dissipationless edge state transport by increasing in-plane magnetic field. The converted σ_{xy} and σ_{xx} shown in Figs. 3(c) and 3(d) also display the evolution from a typical QAH behavior to a ZHP state. For each fixed H_z, σ_{xy} gradually deviates from the $C = 1$ plateau and reaches the $C = 0$ plateau with increasing H_x. The plateau transition is smooth and broad, and the H_x scale increases with H_z value. Moreover, a $\sigma_{xx} \sim 0.5\ e^2/h$ peak emerges near the middle of the transition, as marked by the dashed lines in Figs. 3(c) and 3(d), and the peak occurs at a higher H_x scale with increasing H_z.

Based on the experimental results, we can construct a complete phase diagram of σ_{xy} and σ_{xx} in the $\mu_0H_x - \mu_0H_z$ plane. As shown in Fig. 4(a), the σ_{xy} map is divided into three phases with different Chern numbers. The $C = 0$ and $C = \pm 1$ phases in Fig. 4(b) both have zero σ_{xx}, and they are

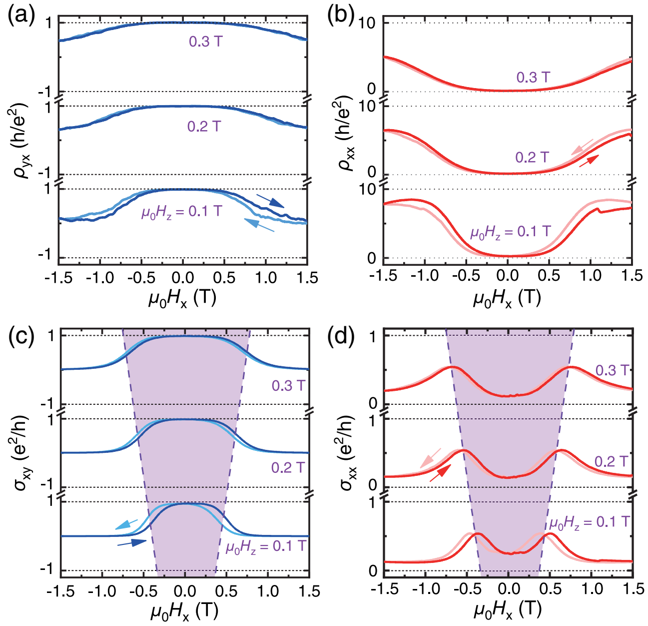

FIG. 3. The in-plane field $\mu_0 H_x$ sweeps of (a) Hall resistivity ρ_{yx}, (b) longitudinal resistivity ρ_{xx}, (c) Hall conductivity σ_{xy}, and (d) longitudinal conductivity σ_{xx} at fixed $\mu_0 H_z = 0.1$, 0.2, and 0.3 T, respectively. The light purple areas in (c) and (d) denote the peak position of σ_{xx}, corresponding to the middle of the $C = 1$ to ZHP transition.

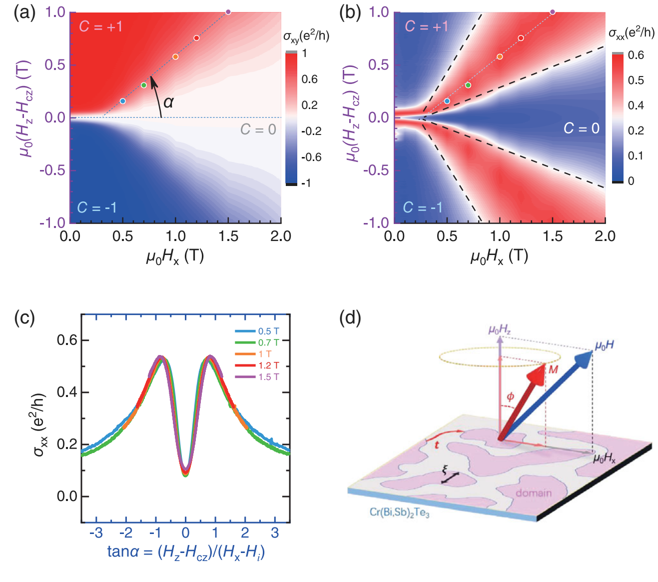

FIG. 4. (a),(b) The color maps of σ_{xy} and σ_{xx} in the H_x-H_z plane. The middle of the $C = 0$ to $C = \pm 1$ plateau transition with $\sigma_{xx} \sim 0.5\ e^2/h$ are marked by the colored dots. (c) Field sweeps of σ_{xx} with respect to $\tan\alpha = (H_z\text{-}H_{cz})/(H_x\text{-}H_i)$, where α is the geometric angle defined in (a) and $\mu_0 H_i = 0.28$ T is the intercept value in Fig. 2(f). All the data collapse into a single curve. (d) Schematic drawing shows the magnetization M and domain structure in the QAH film in the presence of both H_x and H_z.

separated by a red zone with finite σ_{xx}, namely bulk metallic regime. With increasing H_x, the transition area becomes wider, indicating the broadening of the quantum critical region. To reveal the quantum criticality, in Fig. 4(a) we define a geometric parameter α by connecting the points corresponding to the center of the transition with a peak $\sigma_{xx} \sim 0.5\ e^2/h$. The physical meaning of α is $\tan\alpha = (H_z - H_{cz})/(H_x - H_i)$, where $\mu_0 H_i = 0.28$ T is the onset H_x in Fig. 2(f). In Fig. 4(c) the H_z sweeps of σ_{xx} can be plotted as a function of $\tan\alpha$, and they all collapse into a single curve. This behavior strongly resembles the quantum criticality of quantum Hall plateau-plateau transitions observed in high magnetic fields [38–41].

The systematic control of ZHP by H_x provides new clues for understanding the unique physics related to the interplay of magnetism and topology in a QAH insulator. The first finding is the decrease of H_{cz} with increasing H_x, as summarized in Fig. 2(c). The suppression of perpendicular coercive field by in-plane magnetic field has been previously reported in multilayer magnetic microstructures due to the Dzyaloshinskii-Moriya interaction induced magnetization tilt near sample edges, in which the tilt angle is affected by the in-plane field [42,43]. In magnetic TI, it has been theoretically pointed out that the exchange-induced single ion magnetic anisotropy is along the perpendicular orientation [44]. We propose that the reduction of H_{cz} here can be described by the Stoner-Wohlfarth model [45], where the coercivity is determined mainly by the Zeeman energy E_Z and magnetic anisotropy energy E_A. Because spin and orbital momentum with a different g factor both contribute to the atomic magnetic moment, an effective g tensor is needed to determine the spectroscopic splitting in E_Z. The domain reversal process of the QAH system is simulated by assuming the coherent rotation of a single domain in a tilt external field with an anisotropic g factor, as described in detail in Supplemental Material [23]. The black dashed line in Fig. 2(c) is the simulated dependence of H_{cz}, which agrees well with the experimental results. The basic physical picture is that the Zeeman energy gain by the tilt of local moment by H_x makes it easier for the domain to overcome the magnetic anisotropy energy cost in the out-of-plane direction, thus decreasing the perpendicular coercivity.

The second finding is the nonmonotonic evolution of ρ_{xx} peak value at coercivity, as summarized in Fig. 2(c). This quantity is sensitive to the topological band structure and magnetic domain structure during domain rotation, and we propose that both of these essential features can be controlled by H_x. Figure 4(d) schematically draws the domain structure of a QAH insulator, in which the domain size is denoted by ξ. For $\mu_0 H_x < 0.7$ T, there is a finite H_{cz} so during domain rotation the z component of magnetization opens a magnetic gap at the Dirac point, and the ρ_{xx} peak value is determined by the quantum tunneling between the chiral edge states enclosing QAH domains. With increasing H_x, the domain size at H_{cz} decreases continuously. Consequently, the transmission amplitude t between neighboring domains drops, and the peak resistivity value keeps increasing. For $\mu_0 H_x$ above 0.7 T, H_{cz} approaches zero and the z component of magnetization becomes so small that the magnetic gap near the Dirac point closes. The surface conductive state starts to appear near H_{cz}, which causes a decrease of peak resistivity. The nonmonotonic behavior of ρ_{xx} peak value thus can be understood as the competition between the out-of-plane magnetization and H_x, one favoring the gapped QAH state while the other favors the gapless metallic state. The conductivity scaling behavior as a function of $\tan\alpha = (H_z - H_{cz})/(H_x - H_i)$ also manifests that the quantum transport properties are controlled by the relative strength of the perpendicular and in-plane magnetic fields.

The accurate control of ZHP in a QAH system significantly advances the search for chiral Majorana modes based on a QAH/SC hybrid system, which occurs in the process of the $C = 1$ to $C = 0$ transition. The in-plane field broadens the ZHP and its transition to the QAH plateau, thus providing a large parameter regime for the chiral topological SC phase to exist. It reduces the H_{cz} level for the ZHP, making it easier for the fragile proximity induced topological SC to survive. For $\mu_0 H_x \sim 0.5$ T [Fig. 2(d)], the system reaches a quite ideal situation where both the $C = 1$ and $C = 0$ plateaus are well developed, and the broad transition between them occurs for $\mu_0 H_z \sim 0.2$ T. Or as shown in Fig. 3(c), we can apply a small H_z and use H_x as the tuning parameter for the plateau transition, which is known to have much weaker suppression of two-dimensional superconductivity [46–48]. Therefore, applying an in-plane magnetic field is beneficial for realizing the chiral Majorana modes, although the total magnetic field may exceed the H_{cz} under $H_x = 0$.

In conclusion, we demonstrate systematic control of the ZHP in a QAH system by an in-plane magnetic field due to the intricate interplay of magnetism and topological transport properties. With increasing H_x, the ZHP occurs at a lower H_{cz}, with a wider plateau, and a smoother transition to the QAH state. All these features are strongly beneficial for searching the chiral Majorana modes for a QAH in close proximity to an s-wave superconductor.

This work is supported by the Basic Science Center Project of NSFC (Grant No. 52388201), the Innovation Program for Quantum Science and Technology (Grant No. 2021ZD0302502), National Key R&D Program of China (Grants No. 2018YFA0307100 and No. 2018YFA0305603), and NSFC Grants No. 61874172 and No. 11904230. X. F. K. acknowledges the support from the Shanghai Rising-Star program (Grant No. 21QA1406000). This work is supported in part by the Beijing Advanced Innovation Center for Future Chip (ICFC) and the Tencent Foundation.

[*]These authors contributed equally to this work.
[†]kouxf@shanghaitech.edu.cn
[‡]yayuwang@tsinghua.edu.cn

[1] R. Yu, W. Zhang, H.-J. Zhang, S.-C. Zhang, X. Dai, and Z. Fang, Quantized anomalous Hall effect in magnetic topological insulators, Science **329**, 61 (2010).
[2] C.-Z. Chang *et al.*, Experimental observation of the quantum anomalous Hall effect in a magnetic topological insulator, Science **340**, 167 (2013).
[3] K. He, Y. Wang, and Q.-K. Xue, Quantum anomalous Hall effect, Natl. Sci. Rev. **1**, 38 (2014).
[4] H. Weng, R. Yu, X. Hu, X. Dai, and Z. Fang, Quantum anomalous Hall effect and related topological electronic states, Adv. Phys. **64**, 227 (2015).
[5] J. Wang, B. Lian, and S.-C. Zhang, Quantum anomalous Hall effect in magnetic topological insulators, Phys. Scr. **2015**, 014003 (2015).
[6] C.-X. Liu, S.-C. Zhang, and X.-L. Qi, The quantum anomalous Hall effect: Theory and experiment, Annu. Rev. Condens. Matter Phys. **7**, 301 (2016).
[7] C.-Z. Chang, C.-X. Liu, and A. H. MacDonald, Quantum anomalous Hall effect, Rev. Mod. Phys. **95**, 011002 (2023).
[8] J. T. Chalker and P. D. Coddington, Percolation, quantum tunnelling and the integer Hall effect, J. Phys. C **21**, 2665 (1988).
[9] J. Wang, B. Lian, and S.-C. Zhang, Universal scaling of quantum Anomalous Hall plateau transition, Phys. Rev. B **89**, 085106 (2014).
[10] Y. Feng *et al.*, Observation of the Zero Hall Plateau in a Quantum Anomalous Hall Insulator, Phys. Rev. Lett. **115**, 126801 (2015).
[11] X. Kou *et al.*, Metal-to-insulator switching in quantum anomalous Hall states, Nat. Commun. **6**, 8474 (2015).
[12] R. Yoshimi, K. Yasuda, A. Tsukazaki, K. S. Takahashi, N. Nagaosa, M. Kawasaki, and Y. Tokura, Quantum Hall states stabilized in semi-magnetic bilayers of topological insulators, Nat. Commun. **6**, 8530 (2015).
[13] M. Mogi, M. Kawamura, R. Yoshimi, A. Tsukazaki, Y. Kozuka, N. Shirakawa, K. S. Takahashi, M. Kawasaki, and Y. Tokura, A magnetic heterostructure of topological insulators as a candidate for an axion insulator, Nat. Mater. **16**, 516 (2017).
[14] M. Mogi, M. Kawamura, A. Tsukazaki, R. Yoshimi, K. S. Takahashi, M. Kawasaki, and Y. Tokura, Tailoring tricolor structure of magnetic topological insulator for robust axion insulator, Sci. Adv. **3**, eaao1669 (2017).
[15] C. Liu *et al.*, Magnetic-field-induced robust zero Hall plateau state in $MnBi_2Te_4$ Chern insulator, Nat. Commun. **12**, 4647 (2021).
[16] J. Wang, Q. Zhou, B. Lian, and S.-C. Zhang, Chiral topological superconductor and half-integer conductance plateau from quantum anomalous Hall plateau transition, Phys. Rev. B **92**, 064520 (2015).
[17] Q. L. He *et al.*, Chiral majorana edge state in a quantum anomalous Hall insulator-superconductor structure, arXiv:1606.05712.
[18] W. Ji and X.-G. Wen, $1/2\ e^2/h$ Conductance Plateau without 1D Chiral Majorana Fermions, Phys. Rev. Lett. **120**, 107002 (2018).

[19] Y. Huang, F. Setiawan, and J. D. Sau, Disorder-induced half-integer quantized conductance plateau in quantum anomalous Hall insulator-superconductor structures, Phys. Rev. B **97**, 100501(R) (2018).
[20] M. Kayyalha *et al.*, Absence of evidence for chiral majorana modes in quantum anomalous Hall-superconductor devices, Science **367**, 64 (2020).
[21] X. Kou *et al.*, Scale-Invariant Quantum Anomalous Hall Effect in Magnetic Topological Insulators beyond the Two-Dimensional Limit, Phys. Rev. Lett. **113**, 137201 (2014).
[22] Y. Ji *et al.*, Thickness-driven quantum anomalous Hall phase transition in magnetic topological insulator thin films, ACS Nano **16**, 1134 (2022).
[23] See Supplemental Material at http://link.aps.org/supplemental/10.1103/PhysRevLett.130.186201 for addition information of calibration and simulation of coherent rotation, (which includes Refs. [24–36]).
[24] M. Kawamura, M. Mogi, R. Yoshimi, A. Tsukazaki, Y. Kozuka, K. S. Takahashi, M. Kawasaki, and Y. Tokura, Topological quantum phase transition in magnetic topological insulator upon magnetization rotation, Phys. Rev. B **98**, 140404(R) (2018).
[25] M. Kawamura, M. Mogi, R. Yoshimi, A. Tsukazaki, Y. Kozuka, K. S. Takahashi, M. Kawasaki, and Y. Tokura, Current scaling of the topological quantum phase transition between a quantum anomalous Hall insulator and a trivial insulator, Phys. Rev. B **102**, 041301(R) (2020).
[26] C. Tannous and J. Gieraltowski, The Stoner-Wohlfarth model of ferromagnetism, Eur. J. Phys. **29**, 475 (2008).
[27] S. Chikazumi, C. D. Graham, and S. Chikazumi, *Physics of Ferromagnetism*, 2nd ed (Clarendon Press; Oxford University Press, Oxford, New York, 1997).
[28] J. M. Coey, *Magnetism and Magnetic Materials* (Cambridge University Press, Cambridge, England, 2010).
[29] S. J. Blundell, *Magnetism in Condensed Matter* (Oxford University Press, Oxford, New York, 2001).
[30] Q. Liu, C.-X. Liu, C. Xu, X.-L. Qi, and S.-C. Zhang, Magnetic Impurities on the Surface of a Topological Insulator, Phys. Rev. Lett. **102**, 156603 (2009).
[31] G. van der Laan, Microscopic origin of magnetocrystalline anisotropy in transition metal thin films, J. Phys. Condens. Matter **10**, 3239 (1998).
[32] B. Dieny and M. Chshiev, Perpendicular magnetic anisotropy at transition metal/oxide interfaces and applications, Rev. Mod. Phys. **89**, 025008 (2017).
[33] J. Alonso, J. M. Barandiarán, L. Fernández Barquín, and A. García-Arribas, Chapter 1: Magnetic Nanoparticles, Synthesis, Properties, and Applications, in *Magnetic Nanostructured Materials*, edited by A. A. El-Gendy, J. M. Barandiarán, and R. L. Hadimani (Elsevier, Amsterdam, 2018), pp. 1–40.
[34] Z. Wen-Chen, Anisotropy of the g factor for Ni^{2+} and Ni^{3+} ions in the tetragonal phase of $SrTiO_3$, Physica B (Amsterdam) **198**, 329 (1994).
[35] N. Tanaka, Y. Hirota, and K. Motizuki, Anisotropy of g-factor of Cu^{2+} ion and anisotropic exchange interaction between spins in antiferromagnetic Bi_2CuO_4, Czech. J. Phys. **46**, 1847 (1996).
[36] A. Wolos *et al.*, G-factors of conduction electrons and holes in Bi_2Se_3 three-dimensional topological insulator, Phys. Rev. B **93**, 155114 (2016).
[37] C. Liu *et al.*, Distinct Quantum Anomalous Hall Ground States Induced by Magnetic Disorders, Phys. Rev. X **10**, 041063 (2020).
[38] H. P. Wei, D. C. Tsui, M. A. Paalanen, and A. M. M. Pruisken, Experiments on Delocalization and University in the Integral Quantum Hall Effect, Phys. Rev. Lett. **61**, 1294 (1988).
[39] B. Huckestein, Scaling theory of the integer quantum Hall effect, Rev. Mod. Phys. **67**, 357 (1995).
[40] S. L. Sondhi, S. M. Girvin, J. P. Carini, and D. Shahar, Continuous quantum phase transitions, Rev. Mod. Phys. **69**, 315 (1997).
[41] M. Hilke, D. Shahar, S. H. Song, D. C. Tsui, Y. H. Xie, and D. Monroe, Experimental evidence for a two-dimensional quantized Hall insulator, Nature (London) **395**, 675 (1998).
[42] S. Pizzini *et al.*, Chirality-Induced Asymmetric Magnetic Nucleation in $Pt/Co/AlO_x$ Ultrathin Microstructures, Phys. Rev. Lett. **113**, 047203 (2014).
[43] D.-S. Han *et al.*, Asymmetric hysteresis for probing Dzyaloshinskii-Moriya interaction, Nano Lett. **16**, 4438 (2016).
[44] A. S. Núñez and J. Fernández-Rossier, Colossal anisotropy in diluted magnetic topological insulators, Solid State Commun. **152**, 403 (2012).
[45] E. C. Stoner and E. P. Wohlfarth, A mechanism of magnetic hysteresis in heterogeneous alloys, Phil. Trans. R. Soc. A **240**, 599 (1948).
[46] A. M. Toxen, Critical fields of thin superconducting films. I. Thickness effects, Phys. Rev. **127**, 382 (1962).
[47] R. Meservey and P. M. Tedrow, Properties of very thin aluminum films, J. Appl. Phys. **42**, 51 (1971).
[48] P. M. Tedrow and R. Meservey, Critical magnetic field of very thin superconducting aluminum films, Phys. Rev. B **25**, 171 (1982).